Gel electrophoresis of linear and star-branched DNA

Henry W. Lau and Lynden A. Archer*

School of Chemical and Biomolecular Engineering, Cornell University, Ithaca, New York 14853, USA

(Received 5 May 2011; revised manuscript received 6 September 2011; published 22 December 2011)

The electrophoretic mobility of double-stranded DNA in polyacrylamide gel is investigated using an activated hopping model for the transport of a charged object within a heterogeneous medium. The model is premised upon a representation of the DNA path through the gel matrix as a series of traps with alternating large and small cross sections. Calculations of the trap dimensions from gel data show that the path imposes varying degrees of confinement upon migrating analytes, which retard their forward motion in a size-dependent manner. An expression derived for DNA mobility is shown to provide accurate predictions for the dynamics of linear DNA (67–622 bp) in gels of multiple concentrations. For star-branched DNA, the incorporation within the model of a length scale previously proposed to account for analyte architecture [Yuan *et al.*, Anal. Chem. **78**, 6179 (2006)] leads to mobility predictions that compare well with experimental results for a wide range of DNA shapes and molecular weights.

DOI: 10.1103/PhysRevE.84.061916 PACS number(s): 87.15.Tt, 82.45.Tv, 87.15.hj, 82.70.Gg

I. INTRODUCTION

Polymeric matrices such as agarose gels and cross-linked polyacrylamide (PA) networks have long been used to effect the size-based separation of DNA. During electrophoresis, negatively charged DNA fragments are driven by the applied electric field to migrate in a size-dependent manner through pore spaces that are defined by the polymer strands. Absent specific interactions between the DNA and the matrix constituents, the mechanism by which a DNA molecule migrates through the matrix is set primarily by the size of the molecule relative to the size of the openings or pores that are present within the matrix [1]. Thus, the ill-defined internal structure that characterizes a heterogeneous medium like polyacrylamide gel has traditionally hampered the development of theoretical models for DNA gel electrophoresis.

Practical deficiencies associated with slab gels, such as low throughput and high consumable volumes, have motivated a great deal of research on the use of artificial micro- and nanoscale structures for electrophoretic separation of biomolecules [2–4]. Standard lithographic techniques enable precise control over the size, spacing, and arrangement of these structures during the fabrication process, resulting in model gels whose internal sieving environments are more amenable to theoretical examination. A simple geometry that has been the focus of recent experimental, computational, and theoretical studies is the slit-well or the nanoslit array [2,4,5], in which lithographically synthesized obstacles in a fluidic channel allow the cross section to be manipulated periodically in the direction of analyte motion. In one configuration, thin nanosized slits connecting deeper wells in a regular array are believed to impede motion by polyelectrolytes by restricting their orientational, configurational, or conformational freedom. Recently, an activated hopping model has been developed to rationalize the electrophoretic dynamics of DNA in nanoslit arrays [5]. Treating the escape over the entropic barrier imposed by the reduced cross section of a single thin slit as an Arrhenius process, the resulting model correctly predicts the variation in the elution order of DNA at increasing applied fields.

The basic geometrical structure of the nanoslit array conjures obvious similarities to early models for polymer migration in heterogeneous, entangled solutions, melts, and gels [6], implying that the same framework is useful for understanding electrophoresis in more commonly used platforms, such as gels [7]. A recent example of this approach can be found in the work of Shi *et al.* [8], which analogizes the migration path of DNA in a gel to a "pseudonanofilter" whose pores vary in size according to a Gaussian distribution. When gel characterization data for each gel formulation, in the form of a mean pore size and variance, are used as input to the transport model, experimental mobility data were fitted well by this model.

Although the random nature of cross-linked polyacrylamide gels dictates the presence of a distribution of pore sizes, the bimodal nature of this distribution suggests that a thermal activation approach in describing DNA electrophoresis through pores of two mean sizes may provide a good foundation for understanding electrophoresis in these gels. Formed by free radical copolymerization of acrylamide monomers and *bis*-acrylamide cross-linkers, polyacrylamide gels are known to possess local heterogeneities that reflect *bis*-acrylamide's higher reactivity with itself than with the acrylamide comonomer [1,9–14]. Whereas *bis*-rich nodules comprise small pores whose diameters are on the order of nanometers, the large cavities that are connected by these small pores are at least submicrometer in size. Thus, the path taken by a DNA molecule as it is driven through a PA gel during electrophoresis must involve passage through regions that alternate between weakly and strongly confining, corresponding respectively to the large cavities and small pores that are present within the network (Fig. 1). This similarity between the confinement geometry found in a chemically synthesized polyacrylamide gel and a fabricated slit-well array suggests that a theoretical approach, which provides qualitatively accurate predictions about the dynamics of DNA in the latter system should be applicable to the former. In addition, such an approach would allow previously reported relationships between pore sizes and PA concentration [15,16]

*laa25@cornell.edu

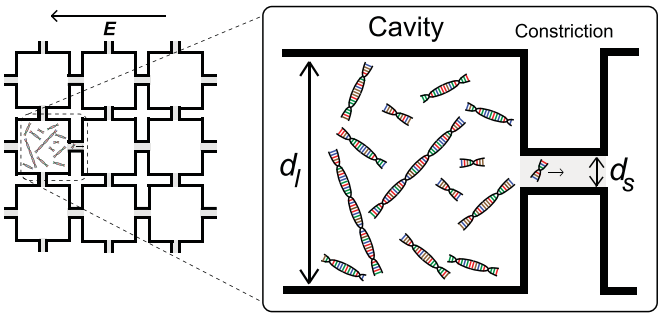

FIG. 1. (Color online) Schematic representation of the internal structure of polyacrylamide gel as a series of large, open cavities of size d_l connected by small constrictions of d_s, which act as entropic barriers to DNA transport in response to applied electric field.

to be directly applied in estimating the internal pore volume, obviating the need for a case-by-case characterization of the sieving matrix as in Ref. [8]. For the present work, we propose and evaluate such an activated transport model for the electrophoresis of linear and star-branched double-stranded DNA in polyacrylamide gels.

II. MATERIAL AND METHODS

A. Polyacrylamide gel synthesis

40% (w/v) acrylamide: *N*,*N*′-methylenebisacrylamide (*bis*-acrylamide) monomer stock solution was made by dissolving commercially available 19:1 weight ratio acrylamide: *bis*-acrylamide powder blend with deionized H_2O. Gels of varied concentration (i.e., the combined weight of acrylamide and *bis*-acrylamide per total volume) were prepared by mixing appropriate volumes of the monomer stock with 3.5 ml ethylene glycol and 0.4 ml 10 × TAE [0.4 M Tris-acetate, 10 mM ethylenediamine tetra-acetic acid (EDTA)], with the final polymerization reaction volume adjusted to 40 ml with deionized water. After the addition of 21 μL *N*,*N*,*N*′,*N*′-tetramethylethylenediamine (TEMED) catalyst and 300 μL of 10% w/v aqueous solution of ammonium persulfate initiator to the reaction volume, the final reaction mixture was swiftly transferred to vertical gel sandwiches that were assembled according to the manufacturer's instructions. All gels were allowed to cast for 2 h to ensure completion of the cross-linking process [17] and were preelectrophoresed for 1 h at 18.5 V/cm before insertion of DNA into sample wells. Reagents were purchased from Sigma (St. Louis, MO, USA).

B. DNA sample preparation

A linear double-stranded DNA size ladder containing fragments up to 622 bp in length was prepared by diluting MspI digest of pBR322 DNA (New England Biolabs, Ipswich, MA, USA) to 500 μg/ml with 1X TE (10 mM Tris-HCl, 1 mM EDTA). Linear and branched DNA structures of total sizes 60, 105, 120, and 180 bp were synthesized according to [17]. For both the DNA ladder and each of the individual branched DNA samples, the dimeric intercalating cyanine dye YOYO-1 (Invitrogen, Carlsbad, CA, USA) was added to 100 μL of stock solution at a 5:1 base pair-to-dye ratio and incubated at 50 °C for more than 2 h in order to minimize band splitting and to promote the homogeneous distribution of dye among the DNA fragments [18].

C. Electrophoresis conditions

Slab-gel electrophoresis was performed using a standard dual cooled SE 600 Chroma gel electrophoresis unit from Hoefer (Holliston, MA, USA), with the heat exchanger for the buffer reservoir connected to an external circulator bath (Thermo NESLAB). All experiments were performed at 9.5 °C, using an applied electric field strength of 18.5 V/cm, and with 0.1X TAE as running buffer, obtained via dilution of 10X TAE with deionized water. At the end of each experiment, gels were illuminated using a Spectroline Select UV transilluminator and recorded with a digital camera (Kodak DC290) present as part of an EDAS 290 gel documentation system from Kodak (Geneva, NY, USA)

D. Mobility calculation and analysis

Intensity profiles for the gel images were extracted using the commercial image analysis software IMAGE PRO PLUS. Band migration distance d was determined as the center of Gaussian peaks fitted to the intensity profile, while error bars are given by the full width at half maximum. Mobility values for each band were computed from the migration distance via $\mu = d/t_{\text{app}}E_{\text{app}}$, where t_{app} is the duration of the experiment and E_{app} is the applied field. Fitting of the model to experimental data, which provides best-fit values of the parameter α, was performed according to a Levenberg-Marquardt nonlinear regression algorithm.

III. RESULTS AND DISCUSSION

A. Model development

As in Ref. [5], the electrophoretic migration of DNA in a cross-linked polyacrylamide network is treated as a thermally activated escape process. Here, the charged analytes move through a series of large cavities of size d_l that are connected by small constrictions of size d_s (Fig. 1). The rate at which an analyte migrates through a single cavity-constriction pair can be written as

$$k = A \exp\left(\frac{-\Delta G}{k_b T}\right), \tag{1}$$

where k_b is Boltzmann's constant, T is the temperature in Kelvin, ΔG is the energetic barrier for the process, and A is the attempt frequency for barrier crossing. For field-mediated motion within the cavity-constriction pair (Fig. 1), ΔG can be separated into an electrostatic (ΔG_E) and an entropic (ΔG_S) component. The work associated with the motion of a negatively charged DNA from the center of a cavity into the center of a constriction in response to an applied field (E_{app}) is given by

$$\Delta G_E = Q_{\text{DNA}} E_{\text{app}}(d_l + d_s)/2, \tag{2}$$

where Q_{DNA} is the effective charge of the DNA. It should be noted that, unlike the case for a nanoslit array, the electric field here is assumed to be unperturbed by the sieving structure. The

entropic contribution to the energetic barrier ΔG_S is obtained via

$$\Delta G_S = -T\Delta S = -k_b T \ln\left(\frac{K_s}{K_l}\right). \tag{3}$$

The partition coefficients for the cavity (K_l) and constriction (K_S) are computed according to [19] by treating them as pores of cubic cross sections. The dimensions of these pores are given by

$$d_s = 1.26c^{-0.64}, \quad \text{Ref. [15]}, \tag{4a}$$
$$d_l = 148c^{-0.58}, \quad \text{Ref. [16]}, \tag{4b}$$

where c represents the concentration (w/v) of the polyacrylamide gel. The attempt frequency A for an analyte of translational diffusion constant D is taken to be the inverse diffusion time from the cavity center to the opening of the constriction:

$$A \approx \frac{D}{(d_1/2)}. \tag{5}$$

Combining Eqs. (1)–(5) and accounting for the negative charge of DNA yields

$$k = \frac{4D}{d_l^2}\exp\left[\frac{|Q_{\mathrm{DNA}}|E_{\mathrm{app}}(d_l+d_s)}{2k_bT} + \ln\left(\frac{K_s}{K_l}\right)\right]. \tag{6}$$

In a slab-gel experiment conducted under snapshot imaging mode (i.e., results are taken by imaging the entire gel after a fixed duration [20]), the mobility μ of a particular analyte is given by the migration distance x of its corresponding band and the duration of the experiment t_{app} (i.e., time over which E_{app} is applied) via

$$\mu = \frac{x}{t_{\mathrm{app}}E_{\mathrm{app}}}. \tag{7}$$

Physically, t_{app} is the sum of the minimum time t_{free} required for an analyte to travel through distance x in free solution and the time t_{act} spent negotiating the N cavity-constriction pairs that form its path through the gel. t_{free} can be rewritten in terms of the free solution mobility μ_0,

$$t_{\mathrm{free}} = \frac{x}{\mu_0 E_{\mathrm{app}}}, \tag{8}$$

while t_{act} can be expressed in terms of the total number of cavity-constriction pairs and the inverse of the rate of transition k through a single pair:

$$t_{\mathrm{act}} = \frac{N}{\alpha k}. \tag{9}$$

Here, α is a proportionality constant of order one. Since $x \approx N(d_l + d_s)$, the relationship $t_{\mathrm{app}} = t_{\mathrm{free}} + t_{\mathrm{act}}$ can be rewritten and combined with Eq. (7) to yield an expression for the reduced gel electrophoretic mobility for a particular species:

$$\mu_r = \frac{\mu}{\mu_0} = \frac{1}{1+\mu_0 E_{\mathrm{app}}/\alpha k} = \frac{1}{1+\mu_0 E_{\mathrm{app}}/\alpha\left(\frac{4D}{d_l^2}\right)(d_l+d_s)\exp\left[\frac{|Q_{\mathrm{DNA}}|E_{\mathrm{app}}(d_l+d_s)}{2k_bT} + \ln\left(\frac{K_s}{K_l}\right)\right]}. \tag{10}$$

B. Model validation—Linear DNA

Using Eq. (10) to predict mobility values for linear DNA fragments within polyacrylamide gel matrices requires inputs such as the size, charge, and the diffusion coefficient of each fragment. For DNA fragments containing M base pairs, the mean squared radius of gyration is computed using the Benoit-Doty expression [21] for the Kratky-Porod wormlike chain model [22],

$$\langle R_g^2\rangle = \frac{R_{\max}b_k}{6}\left\{1 - 3\left(\frac{b_k}{2R_{\max}}\right) + 6\left(\frac{b_k}{2R_{\max}}\right)^2 - 6\left(\frac{b_k}{2R_{\max}}\right)^3\left[1 - \exp\left(-\frac{2R_{\max}}{b_k}\right)\right]\right\}, \tag{11}$$

where the contour length is given as $R_{\max} = Mb$, and the Kuhn step size b_k and monomer size b were taken to be 124 and 0.42 nm, respectively. These values account for the 24% increase in persistence length and contour length that is known to result from the use of YOYO-1 as intercalating labels [23]. The effective charge of DNA Q_{DNA} is computed using the formula $Q_{\mathrm{DNA}} = qM(1-\theta)$, where q is the charge per base pair owing to the presence of bare phosphate residues, and θ is the fraction of phosphate charges that are expected to be neutralized by condensed counterions. The value of θ is approximated via counterion condensation theory to be 74% for monovalent counterions at the experimental temperature [24]. The translational diffusion coefficient for each DNA size was calculated based on the work of Ortega *et al.* on the hydrodynamic properties of rod- and disklike particles of length L, diameter d, and aspect ratio $p = L/d$ in a solvent of viscosity η [25]:

$$D_t = \frac{k_bT}{6\pi\eta LC_i}\left(\frac{16p^2}{3}\right)^{1/3}, \tag{12a}$$

$$C_i = 1.009 + 1.395\times10^{-2}(\ln\ p) + 7.880\times10^{-2}(\ln\ p)^2 + 6.040\times10^{-3}(\ln\ p)^3. \tag{12b}$$

By taking the 67-bp fragment as a reference band, model predictions for gel mobility are obtained using the formula

$$\mu = \mu_{67}\frac{\mu_{r,M}}{\mu_{r,67}}, \tag{13}$$

where μ_{67} is the measured mobility for the 67-bp fragment, and $\mu_{r,M}$ and $\mu_{r,67}$ are the theoretical reduced mobility values calculated via Eq. (10) for DNA fragments of size M and 67 bp, respectively. Theoretical curves are constructed by fitting Eq. (13) to experimental data while treating α as a freely adjusted parameter.

Figure 2 shows gel mobility values for 4%, 7.5%, and 10% polyacrylamide gel plotted as a function of DNA size. In general, the model is seen to provide predictions for DNA mobility that compare well with measurement values. Across

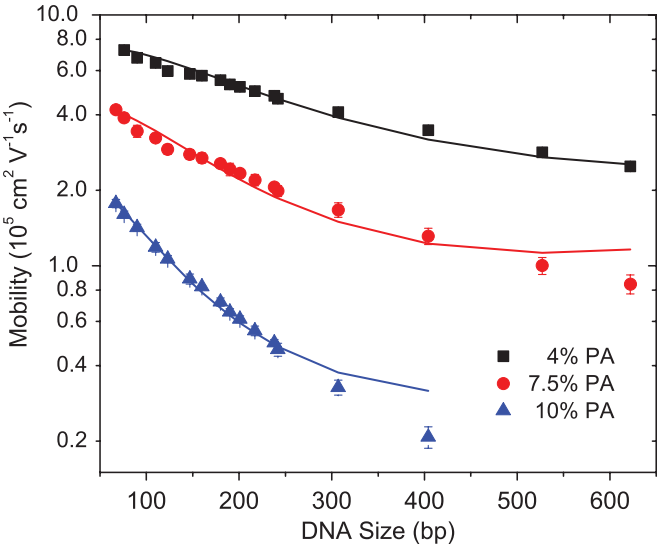

FIG. 2. (Color online) Gel mobility plotted as a function of DNA fragment size for $c = 4\%$ (squares), 7.5% (circles), and 10% (triangle) PA gels. Curves are theoretical predictions computed using Eqs. (10) and (13), with $\alpha = 0.75$, 0.50, and 0.22 for the three concentrations, respectively.

all gel concentrations considered, the size dependence of mobility is correctly captured by the model, suggesting that the key physics underlying DNA transport through the polymer network has been adequately addressed. The onset of deviation between prediction and data appears to correlate with analyte sizes which approach or exceed the cavity dimension d_l of each concentration. This is shown by a plot of $R_g/d_l(c)$ versus DNA size (Fig. 3), where DNA sizes which correspond to $R_g/d_l \sim 1$ for 7.5% and 10% PA gels also marks where the theoretical curves begin to depart from experimental values in Fig. 2. For the 4% PA gel, the DNA size for which R_g/d_l is greater than unity exceeds the largest fragment size investigated, leading

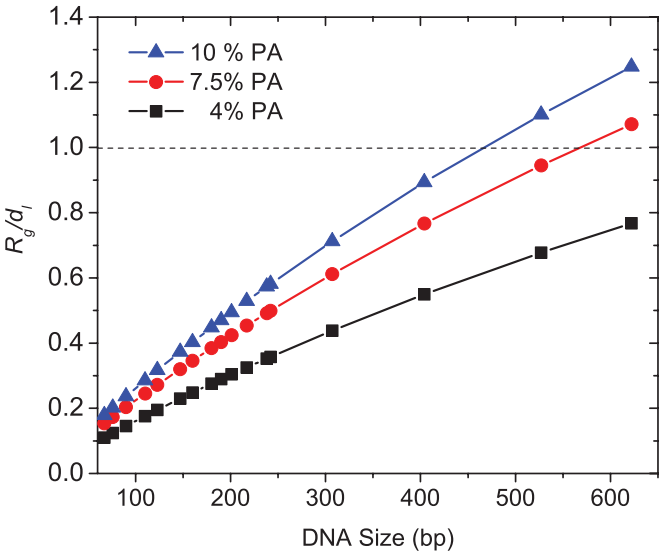

FIG. 3. (Color online) $R_g/d_l(c)$ plotted against DNA size for $c = 4\%$ (squares), 7.5% (circles), and 10% (triangle) PA gels. Dotted line at $R_g/d_l = 1$ is added to guide the eye.

to quantitative agreement between theory and data throughout the entire size range studied. The breakdown of our model at increasing DNA size for select concentrations of PA can thus be attributed to the onset of non-Ogston modes of electrophoretic transport for persistence chains [3].

First introduced as a dimensionless constant of proportionality between the rate of transition through a single constriction-cavity pair and the inverse trapping or activation time for a molecule attempting passage (see Sec. III A), the parameter α also appears as a prefactor for the attempt frequency [cf. Eqs. (6) and (10)], which provides a way to assess the accuracy of the latter. For example, α values of less than unity indicate overpredictions of the attempt frequency, which may occur from an overestimation of the DNA diffusivities or an underestimation of the matrix pore sizes.

In Fig. 2, decreasing values of α are shown to be required to fit data obtained at higher PA concentrations, indicating that Eq. (12) overestimates the diffusion constants of DNA to a greater degree for denser matrices. Given that the diffusive transport of solutes within a hydrogel is known to be retarded by a combination of hydrodynamic drag and steric obstructions engendered by the polymer strands that constitute the network, our model implicitly neglects the effects of hindered diffusion by estimating DNA diffusivity with Eq. (12), which is derived on the basis of dilute conditions and in free solution [25]. Additionally, the value of α can be interpreted as the ratio of the diffusion constants for hindered and free diffusion (i.e., diffusion in the absence of steric hindrance), which can be estimated using one of many mathematical frameworks proposed to describe hindered diffusion of proteins and other solutes in porous media [26,27]. A comprehensive assessment of all available hindered diffusion models is beyond the scope of our current work.

C. Model extension—Nonlinear DNA

In an effort to evaluate the applicability of the model to describe motion of nonlinear DNA in PA networks, we performed gel electrophoresis of star-branched DNA ranging in total size from 60 to 180 bp. Previous investigations into the gel electrophoresis of star-branched DNA have shown that the use of the radius of gyration to describe analyte size fails to capture the dependence of mobility on analyte architecture. Whereas DNA molecules possessing the same total number of base pairs have been observed to migrate more slowly as their shapes are transformed from a linear molecule to a symmetric star [7,17], the reduction in the gyration radius that corresponds to such a transformation leads to the opposite, and inaccurate, conclusion that the linear molecule should exhibit the lowest mobility.

To account for the observed topology dependence, Yuan *et al.* [7] proposed a length scale based on the concept of the smallest confining cylinder. For star-branched molecules of arbitrary branch location or length, the largest cross section presented by the analyte is taken to be the end-to-end length l_c of the confining cylinder, while its radius a_c is equated to the length of the line drawn perpendicularly from the end point of the shortest arm, to the line connecting the ends of the two

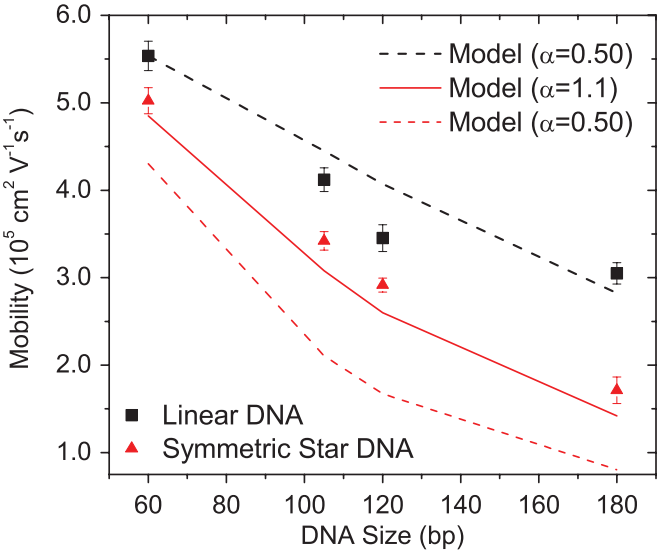

FIG. 4. (Color online) Mobility plotted against DNA size M_{Total}, for linear and symmetric-star-branched DNA containing three arms of length $M_{\text{arm}} = M_{\text{Total}}/3$. Curves represent mobility predictions for linear ($\alpha = 0.50$, black dashed) and branched ($\alpha = 0.50$, red dotted; $\alpha = 1.1$, red solid) analytes.

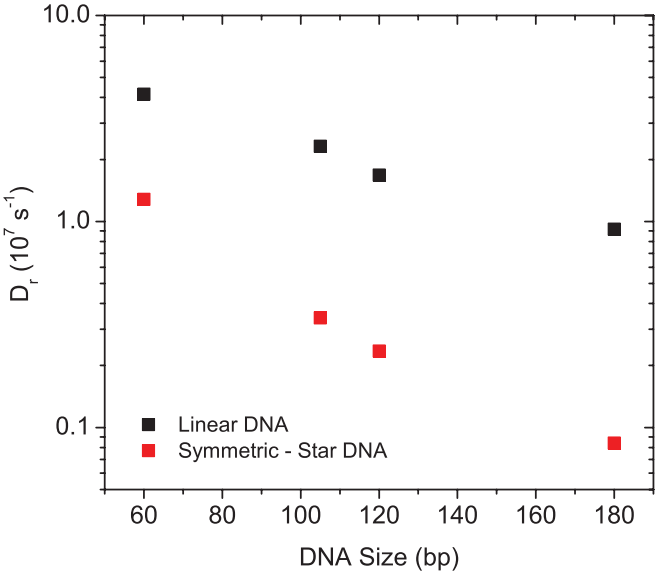

FIG. 5. (Color online) Rotational diffusion constants plotted versus total DNA size for linear and symmetric-star-branched DNA. Note that the y axis is presented in semilogarithmic scale.

larger arms [7]. The radius of gyration of the confining cylinder $R_{g,c}$, calculated via

$$R_{g,c}^2 = \frac{a_c^2}{2} + \frac{l_c^2}{12}, \tag{14}$$

is treated as the characteristic length scale for the nonlinear analytes. In the present contribution, the concept of the smallest confining cylinder is extended to the estimation of the translational diffusivity of the star-branched molecules within the cavity. Values of a_c and l_c associated with each sample are used to compute the aspect ratio of the confining cylinder $p_c = a_c/l_c$, which is then used to estimate D_t via Eqs. (12a) and (12b).

1. Symmetric-star DNA

We begin our analysis of nonlinear DNA by first focusing on three-arm, symmetric stars, i.e., branched DNA fragments of total mass M that possess three arms of equal length $M/3$. Figure 4 shows the electrophoretic mobility of linear DNA and symmetric-star-branched DNA in 7.5% PA as a function of total DNA size. Across all sizes investigated, a linear DNA exhibits a higher mobility value than a symmetric-star-branched DNA of identical total mass, consistent with previous findings [17]. Using Eq. (14) to define analyte size, our model is able to provide mobility predictions that are in good agreement with the observed values for both linear and star DNA.

Our results for the branched DNA also show a stronger dependence on total size than for linear DNA fragments. This observation can be attributed to a combination of steric and hydrodynamic effects induced by the nonlinear architecture of the branched samples. In the context of steric constraints imposed by the gel fibers, the number of orientations that a symmetric-star DNA can assume within a constriction (i.e., small pore) is smaller than that for a linear DNA of identical mass. At the same time, the time scale to achieve these "permissible" orientations via random thermal fluctuations is expected to be longer for symmetric-star DNA. Using the program HYDROSUB [28] to compute the end-over-end rotational diffusivity D_r for both sets of samples, a plot of D_r versus DNA size shows that D_r values for symmetric stars are consistently lower than those for linear DNA (Fig. 5). Furthermore, the rotational diffusivity of star samples exhibits a stronger decline with overall size than their linear counterparts. Requiring symmetric-star DNA of greater mass to take a *longer* time

TABLE I. Total mass, arm dimensions, and $R_{g,c}$ of star-branched DNA molecules.

Total mass (bp)	Length of arm 1 (bp)	Length of arms 2and 3 (bp)	$R_{g,c}$ (nm)
60	10	25	8.5
	14	23	9.0
	20	20	9.9
105	5	50	13.8
	11	47	14.3
	17	44	14.9
	23	41	15.6
	29	38	16.4
	35	35	17.3
120	8	56	16.0
	16	52	16.6
	24	48	17.5
	32	44	18.6
	40	40	19.8
180	10	85	23.8
	20	80	24.6
	30	75	25.6
	40	70	26.8
	50	65	28.2
	60	60	29.7

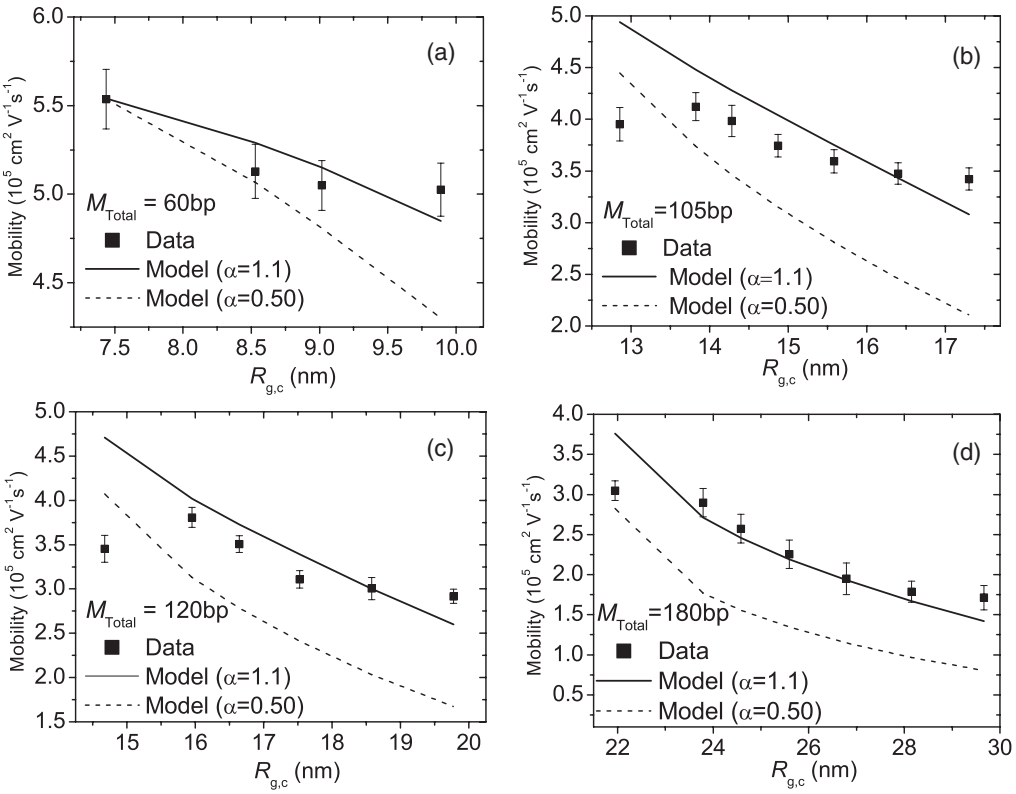

FIG. 6. Mobility of star DNA in 7.5% PA is plotted against effective analyte size, as represented by the radius of the smallest confining cylinder $R_{g,c}$ for DNA samples with total mass of (A) 60 bp, (B) 105 bp, (C) 120 bp, and (D) 180 bp. Theoretical curves [calculated using Eqs. (10) and (13)] corresponding to $\alpha = 0.50$ (Dotted) and $\alpha = 1.1$ (Solid) are also displayed.

to attain a *smaller* number of allowable configurations for passage through the small pores is consistent with the enhanced size dependence that is observed for the nonlinear molecules.

2. *Asymmetric-star DNA*

Intermediate between the linear and symmetric-star DNA architectures are asymmetric-star molecules bearing three arms that are of unequal length. First studied by Heuer *et al.* in Ref. [17], analytes containing an identical number of base pairs (and therefore an identical number of charges) can be synthesized so that their overall shape ranges from a linear rod to a symmetric star. For such a family of molecules, the variations in mobility must reflect the role of shape, rather than of charge, on the molecule's migration within the matrix. Here, electrophoretic measurements for four sets of branched DNA (M_{Total} = 60, 105, 120, and 150 bp; see Table I for analyte details) were conducted in order to gauge the effectiveness of our model in capturing the influence of analyte architecture on mobility. Figure 6 presents the experimental and theoretical values as a function of $R_{g,c}$ [as defined via Eq. (14)]. For all M_{Total}, a shift in the shape of the branched analyte toward that of a symmetric star (i.e., toward increasing values of $R_{g,c}$) leads to a reduction in mobility. Our approach in using $R_{g,c}$ to account for the effect of analyte architecture appears sound, as the resulting theoretical curves exhibit the correct trend and provide reasonable predictions for analyte mobility.

In Fig. 4, the mobility of linear fragments, synthesized separately from the DNA size ladder used for the experiments in Fig. 2, is well described by the model, using the same fitted value of α for the 7.5% PA gel. However, this particular value leads to poor predictions for the mobility of symmetric star DNA, as demonstrated by the dotted curve within the figure. By contrast, an α value closer to unity yields excellent predictions for the mobility of both symmetric and asymmetric DNA stars (solid curves in Figs. 4 and 6). Thus, application of the confining cylinder concept to define the length and aspect ratio of branched samples appears to compensate for the overestimation of analyte diffusivity associated with the use of Eqs. (12a) and (12b). In light of the equality between the reduced diffusivity and the reduced mobility for charged particles at the low field limit [29], the apparent success in using $R_{g,c}$ to estimate the hindered diffusion coefficient of nonlinear DNA is consistent with results in Ref. [7] which show good agreement between data and predictions made via $R_{g,c}$.

IV. CONCLUSION

We have proposed a model for the electrophoresis of DNA in polyacrylamide gels that treats the migration of DNA through the matrix as a series of thermally activated transitions through regions of strong confinement. Using literature results to estimate the dimensions of the cavities and constrictions that define the path of a migrating DNA, our model yields

theoretical curves that match well with data obtained at multiple matrix concentrations. In terms of DNA size, our model can be applied to describe the mobility of analytes that are smaller than the large pores within the gel, i.e., before the expected onset of reptation. By applying the concept of a smallest confining cylinder to define the length scale of star-branched DNA molecules, our model correctly captures the dependence of mobility upon analyte architecture, mass, and charge. Overall, our results demonstrate the versatility of our model in describing the electrophoretic migration of charged molecules possessing arbitrary shape within heterogeneous media.

ACKNOWLEDGMENTS

This paper is based upon work supported by the National Science Foundation, Award No. DMR-1006323. Parts of this work made use of STC shared experimental facilities supported by the National Science Foundation under Agreement No. ECS-9876771.

[1] N. C. Stellwagen and E. Stellwagen, J. Chromatogr. A **1216**, 1917 (2009).
[2] J. Fu, P. Mao, and J. Han, Trends Biotechnol. **26**, 311 (2008).
[3] J. L. Viovy, Rev. Mod. Phys. **72**, 813 (2000).
[4] K. D. Dorfman, Rev. Mod. Phys. **82**, 2903 (2010).
[5] E. A. Strychalski, H. W. Lau, and L. A. Archer, J. Appl. Phys. **106**, 024915 (2009).
[6] M. Muthukumar and A. Baumgartner, Macromolecules **22**, 1937 (1989); **22**, 1941 (1989); A. Hoagland and M. Muthukumar, *ibid.* **25**, 6696 (1992).
[7] C. L. Yuan, E. Rhoades, D. M. Heuer, S. Saha, X. W. Lou, and L. A. Archer, Anal. Chem. **78**, 6179 (2006).
[8] N. Shi and V. M. Ugaz, Phys. Rev. Lett. **105**, 108101 (2010).
[9] A. H. Hecht, R. Duplessix, and E. Geissler, Macromolecules **18**, 2167 (1985).
[10] J. Beselga, J. L. Nieto, I. Hernandez-Fuentes, I. F. Pierola, and M. A. Lorente, Macromolecules **20**, 3060 (1987).
[11] J. G. H. Joosten, J. L. McCarthy, and P. M. Pusey, Macromolecules **24**, 6690 (1991).
[12] J. Beselga, M. A. Lorente, J. L. Nieto, I. Hernandez-Fuentes, and I. F. Pierola, Eur. Polym. J. **24**, 161 (1988).
[13] J. L. Nieto, J. Beselga, I. Hernandez-Fuentes, M. A. Lorente, and I. F. Pierola, Eur. Polym. J. **23**, 551 (1987).
[14] T. P. Hsu and C. Cohen, Polymer **25**, 1419 (1984).
[15] I. H. Park and C. S. Johnson, Macromolecules **23**, 1548 (1990).
[16] N. C. Stellwagen, Electrophoresis **19**, 1542 (1998).
[17] D. M. Heuer, S. Saha, A. T. Kusumo, and L. A. Archer, Electrophoresis **25**, 1772 (2004); D. M. Heuer, C. Yuan, S. Saha, and L. A. Archer, *ibid.* **26**, 64 (2005); D. M. Heuer, S. Saha, and L. A. Archer, Biopolymers **70**, 471 (2003).
[18] C. Carlsson, M. Jonsson, and B. Akerman, Nucleic Acids Res. **23**, 2413 (1995).
[19] J. C. Giddings, E. Kucera, C. P. Russell, and M. N. Myers, J. Phys. Chem. **72**, 4397 (1998).
[20] E. Ribeiro and J. C. Sutherland, Anal. Biochem. **210**, 378 (1993).
[21] H. Benoit and P. Doty, J. Phys. Chem. **57**, 958 (1953).
[22] O. Kratky and G. Porod, Recl. Trav. Chim. Pays-Bas **68**, 1106 (1949).
[23] O. B. Bakajin, T. A. J. Duke, C. F. Chou, S. S. Chan, R. H. Austin, and E. C. Cox, Phys. Rev. Lett. **80**, 2737 (1998).
[24] M. O. Fenley, G. S. Manning, and W. K. Olson, Biopolymers **30**, 1191 (1990).
[25] A. Ortega and J. G. de la Torre, J. Chem. Phys. **119**, 9914 (2003).
[26] B. Amsden, Macromolecules **31**, 8382 (1998); **32**, 874 (1999).
[27] Y. Cu and W. M. Saltzman, Adv. Drug Delivery Rev. **61**, 101 (2009).
[28] J. G. de la Torre and B. Carrasco, Biopolymers **63**, 163 (2002).
[29] J. F. Mercier, G. W. Slater, and H. L. Guo, J. Chem. Phys. **110**, 6050 (1999).